Chapter 6
Computer-Aided Analysis and Design of Wideband Acoustic Devices

6.1 INTRODUCTION

The goal of wideband acoustic design is the introduction of an acoustic signal with high efficiency over as wide a frequency range as possible. The acoustic device is characterized by its electrical impedance, which is a complex function of material constants of the elements that make up the device, and the frequency. Accurate modeling is essential for optimum device design and performance.

Using the acoustic model developed in Chapter 5, we were able to write a closed-form solution for the input impedance characteristic only for the relatively simple structure in which a piezoelectric transducer is rigidly attached to an infinitely long substrate, the ground metalization is neglected, and there is no acoustic attenuation in transducer or substrate. Attempting to develop a closed-form solution for more complex geometries results in greatly increased complexity. In this chapter, we investigate computer-aided techniques to which all the configurations in Figure 5.9 can be adapted. Specifically, we analyze the single transducer structure with finite substrate length in which the ground plane thickness is acoustically significant. We introduce attenuation by allowing the propagation constant to become complex, and we catenate multiple layers of arbitrary acoustic properties by multiplying matrices, each of which represents an individual layer.

Efficient conversion of electrical energy to acoustic energy requires that the device impedance be as close to 50 Ω (the source resistance) as possible. Matching the device is complicated because its resistive component depends on frequency and its reactive component varies with the acoustic parameters of the various layers. We consider some practical cases and show the effects of external matching elements as well as ground plane metalization.

THE SMITH CHART

The Smith chart, shown in Figure 6.1, is an ideal tool for the analysis of acoustic devices. The chart has numerous functions in microwave analysis, but for our purposes it can be considered as a graph of the complex reflection coefficient ρ onto which curves of constant resistance and reactance have been superimposed. Because ρ is complex,

$$\rho = u + jv \tag{6.1}$$

The *normalized* impedance is

$$z = \frac{Z_{in}}{Z_0} = \frac{1 + \rho}{1 - \rho} = r + jx = \frac{1 + (u + jv)}{1 - (u + jv)} \tag{6.2}$$

In (6.2), Z_{in} is the impedance of the acoustic device, which consists of the reactive capacitance of C_0 and the complex Z_a; Z_0 is the source impedance, usually 50 Ω (real). Thus, z is a normalized impedance with real (resistive) and imaginary (reactive) components represented by r and x. Equating the real and imaginary parts of (6.2), we find

$$r = \frac{1 - (u^2 + v^2)}{(1 - u)^2 + v^2} \tag{6.3}$$

$$x = \frac{2v}{(1 - u)^2 + v^2} \tag{6.4}$$

(6.3) can be written in the form:

$$\left(u - \frac{r}{1 + r}\right)^2 + v^2 = \frac{1}{(1 + r)^2} \tag{6.5}$$

Equation (6.5) is the equation of a circle with center at $(r/(r + 1), 0)$ in the u-v coordinate system with radius $1/(r + 1)$. On each of these circles, the normalized resistance is constant. Further, each circle is contained completely with the chart. The outermost circle has radius 1 and is centered at the center of the chart (0, 0). As the resistive component increases, the circles become smaller and their centers move to the right. Equation (6.4) can be written in the form:

$$(u - 1)^2 + \left(v - \frac{1}{x}\right)^2 = \frac{1}{x^2} \tag{6.6}$$

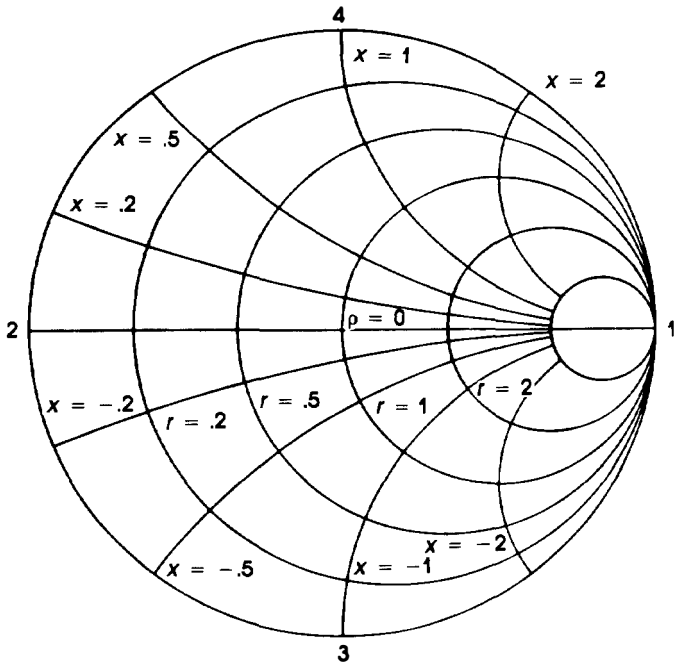

Figure 6.1 The Smith chart. Points 1 and 2 correspond to open and short circuits, and points 3 and 4 represent normalized reactances of -1 and $+1$, respectively. In the center of the chart, the reflection coefficient is zero, and all incident energy is absorbed.

Equation (6.6) represents circles of constant normalized reactance. They are centered outside the chart at $(1, 1/x)$ and have radii of $1/x$.

The center of the chart corresponds to $|\rho| = 0$ (all energy is absorbed by the device), and the outer periphery corresponds to $|\rho| = 1$ (energy is completely reflected by the device). Points 1 and 2 correspond to open ($\rho = +1$) and short ($\rho = -1$) circuits, respectively; points 3 and 4 represent normalized (to 50 Ω) capacitive (negative) and inductive (positive) reactances of unity. All points in the interior of the chart, except the resistive line that connects the open and short, represent complex impedances composed of resistive and reactive components (capacitive in the bottom half, inductive in the top half).

As an example, consider the impedance of a simple capacitor shown in Figure 6.2. The resistance of this device is zero, so its characteristic is represented by the circle of radius 1 centered at (0, 0). At dc, it "looks" like an open (point 1). As frequency increases, the characteristic traverses the outer rim of the chart unit, as $\omega \to \infty$, it approaches a short (point 2).

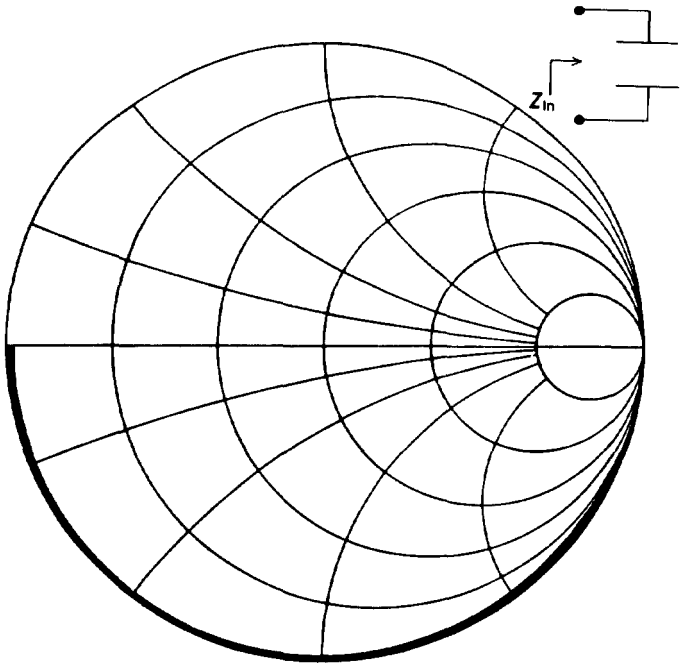

Figure 6.2 Impedance characteristic of a simple capacitor. At dc the circuit is an open, and a frequency increases the circuit becomes a short. The curve traverses the chart clockwise.

Because $|\rho| = 1$ for all frequencies, no power is absorbed. Its impedance characteristic does not cross over to the top (inductive part) of the Smith chart for any frequency. Similarly, an inductor "looks" like a short at dc and an open at very high frequencies and is located only in the top half of the chart; like the capacitor, it absorbs no energy. Both the inductive and capacitive impedance traverse the Smith chart in a clockwise direction as the frequency increases.

A circuit with resistive and reactive components does absorb energy. A simple example is the series combination of a resistor and capacitor. The Smith chart's impedance characteristic for this case is shown in Figure 6.3. We note that as the frequency increases, the curve moves along a circle of constant resistance, given by (6.4). Similarly, the absorbed energy is a function of frequency. At dc, the circuit looks open (and thus $\rho = 1$), and at very high frequencies the circuit looks like a resistor and absorbs maximum energy (because $X_C \rightarrow 0$). Similarly, a circuit consisting of a series combination of an inductance and a resistance looks like a resistance at dc and an open at very high frequencies.

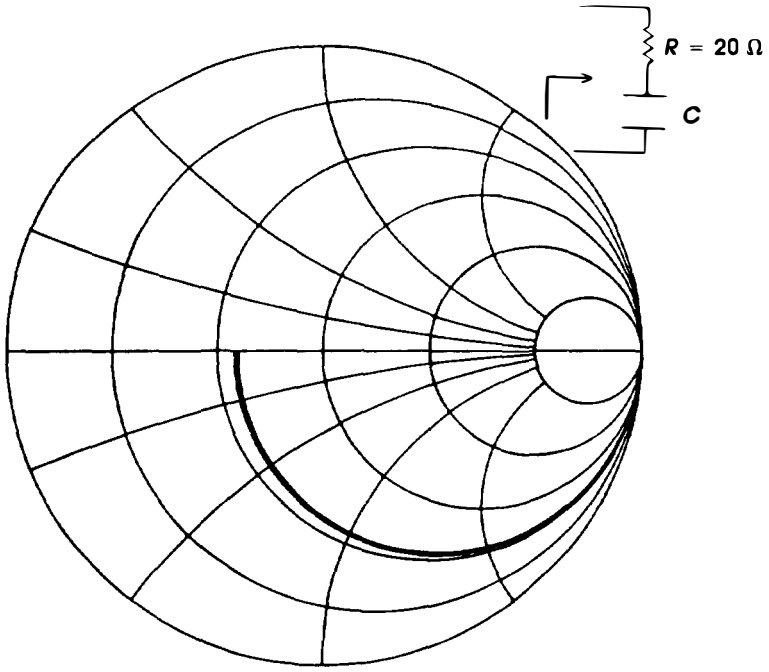

Figure 6.3 Impedance characteristic of a resistor in series with a capacitor. In this case, there is energy absorption.

6.3 RETURN LOSS

The frequency of maximum energy absorption (the point closest to the center of the chart) is not shown explicitly in the Smith chart figures. Although it is possible to place frequency markers on the impedance characteristic, this technique is usually not convenient, especially if the position of the characteristic changes slowly with frequency. To highlight the frequency variation, we use a linear graph of reflection coefficient *versus* frequency, called the return loss (RL) plot, which is shown in Figure 6.4. We derive this curve from the impedance characteristic by using the formula:

$$RL = 20 \log(\rho_r^2 + \rho_i^2) \tag{6.7}$$

where ρ_r and ρ_i are the real and imaginary parts of the reflection coefficient. From (6.7), it is clear that the center of the Smith chart corresponds to an RL that decreases without limit, whereas RL for a pure capacitor or

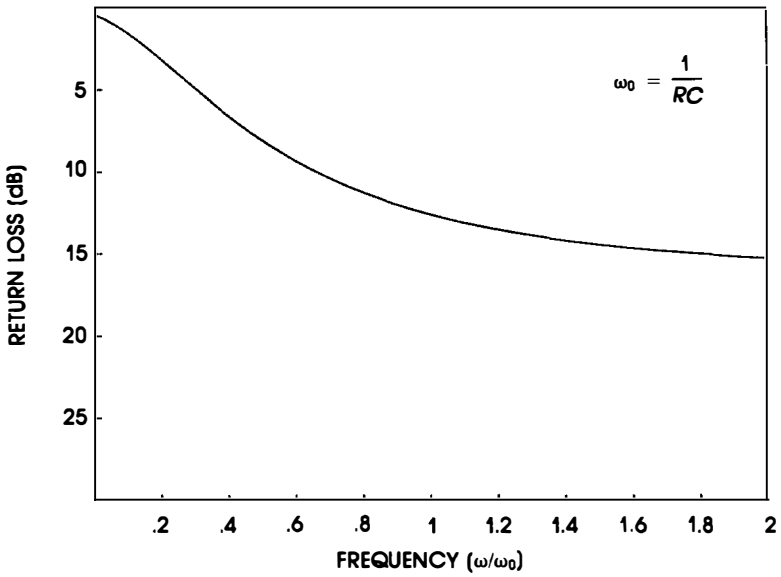

Figure 6.4 Return loss of the resistor-capacitor series combination.

inductor is zero. A return loss of 3 dB means that half the power is absorbed by the device and half is returned to the source. The physical interpretation is that for $|\rho| = 1$ (RL = 0) all energy introduced into the device is "returned" to the source, whereas for $|\rho| = 0$ all the energy is absorbed from the source by the load.

Another important figure of merit is the voltage standing wave ratio (VSWR), defined as

$$\text{VSWR} = \frac{1 + |\rho|}{1 - |\rho|} \tag{6.8}$$

where $1 \leq \text{VSWR} \leq \infty$. A well-matched acoustic device will have a VSWR less than about 1.5, which corresponds to a return loss of less than about 8 dB over the frequency band. Although the RL curve does provide frequency information, it does not differentiate between capacitive or inductive circuits. A complete analysis requires both the Smith chart and RL curves. Return loss curves are measured on a *scalar* network analyzer, and Smith chart curves require the costlier *vector* analyzer for their measurement.

Because the input impedance of acoustic devices contains real and imaginary (usually capacitive) parts, we would expect its characteristic to

bear some resemblance to the circuit of Figure 6.3. However, the resistance is a complicated function of frequency, so the impedance is quite difficult to predict even for the simplest cases. The real and imaginary parts of the impedance have been already calculated for a transducer attached to a substrate infinite length. The complex impedance can be converted to a complex reflection coefficient by using (6.1) and solving for ρ in terms of z_{in}:

$$\rho = \frac{z_{in} - 1}{z_{in} + 1} \tag{6.9}$$

where z_{in} is the normalized input impedance of the acoustic device, (normalized to 50 Ω) composed of the capacitive reactance of C_0 and the acoustic contribution Z_a. In this form, the characteristic can be graphed either on the Smith chart or with RL coordinates.

Example 6.1. Discuss the input impedance for Example 5.3 from its Smith chart characteristic. The Smith chart impedance characteristic using the infinite substrate simplification (5.51) are shown in Figure 6.5 for a lithium niobate 36° $\langle y \rangle$ transducer (longitudinal on $\langle x \rangle$ lithium niobate operating at a center frequency of 2 GHz. The frequency range (not shown on the plot) is from 1 to 3 GHz. Outside this range, the characteristic quickly approaches the outer periphery of the chart. The relevant constants for the two crystal media were given in Example 5.3. As in Example 5.3, the transducer active area is chosen so that at resonance the acoustic radiation impedance is 50 Ω. This is indicated in Figure 6.5 by the fact that the impedance characteristic lies near the $r = 1$ (50 Ω) circle for frequencies close to resonance. The thickness of the transducer is given by the half-wave resonance condition (5.55) and is approximately 1.7 μm. Thus, in the vicinity of resonance (approximately 2 GHz), there is an appreciable amount of energy absorbed by the device, as indicated by the increase in the resistive component of the curve near resonance. Because the model does not include acoustic attenuation in the transducer, all of this energy must be converted into acoustic energy in the substrate. At resonance, the device "looks" like a 50-Ω resistor in series with a capacitor of value

$$C_0 = \frac{\epsilon^S A}{d} = .6 \text{ pF}$$

The capacitor, which is always present, causes a nonzero reflection coefficient, and thus a portion of the electrical power is returned to the source. In this example, the capacitive reactance $1/\omega C_0$ is approximately

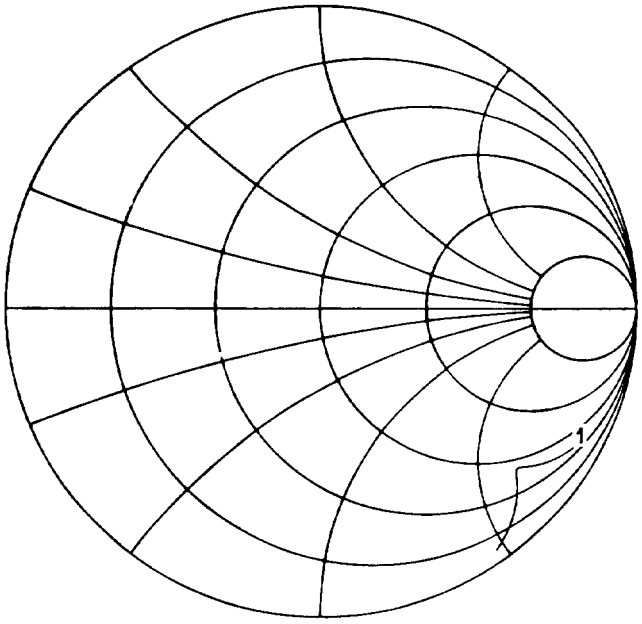

Figure 6.5 Impedance characteristic of longitudinal mode $LiNbO_3$ on $\langle x \rangle$ $LiNbO_3$ with no bond layer. The area is 3×10^{-9} m^2, and the transducer thickness is 1.7 μm. The frequency range is from 1 to 3 GHz.

130 Ω. The normalized value is 2.6, which agrees with the location of the characteristic on the chart. We can reduce ρ to zero by adding a series *inductor* with a value chosen so that at resonance its inductive reactance cancels the capacitive reactance of C_0. Of course, this cancellation is valid only at the resonance frequency, but, at least over a narrow band, it is possible to produce a device in which all the electrical source energy is absorbed. This does not imply that there is 100% conversion of electrical energy into acoustic energy, because some of it may be converted into heat in the transducer. For Example 6.1, the value of inductance is given by (5.61) and is 10 nH.

Figure 6.6 illustrates the effect of the coupling constant on the impedance characteristic. The curves correspond to the configuration of Example 6.1 but with different coupling constants. It is clear that a high coupling constant (curve 2) is desirable for wideband operation. As the coupling constant is reduced, less electrical energy is converted to acoustic energy and the device looks increasingly like a capacitor (i.e., the characteristic lies near the periphery of the lower half of the chart). As k_t^2 is increased, the opposite occurs and the *resistive* component of Z_{in} increases. Just as

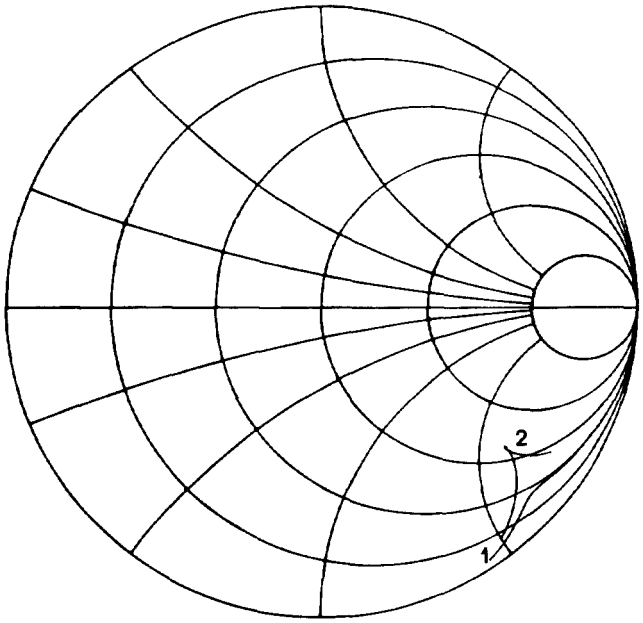

Figure 6.6 Impedance characteristic of the device in Figure 6.5 with varying coupling constant: curve 1, $k_t^2 = .1$; curve 2; $k_t^2 = .4$. Note that the larger k_t^2 results in increased conversion of electric to acoustic energy.

importantly, the characteristic can be more easily designed to be closer to the $r = 1$ circle over a larger frequency band (in this case from 1 to 3 GHz). This behavior increases the bandwidth and facilitates matching. It is consistent with (5.63), in which bandwidth is proportional to k_t^2.

The radiation resistance is required to be close to 50 Ω for efficient energy conversion. For very high frequency operation, design constraints (which we discuss in Chapter 8) may limit $\hat{R}_a$ to only a few ohms. As shown in Figure 6.6, the best way to ensure the largest possible radiation resistance is to use transducers with high coupling constants. The value of $\hat{R}_a$ can also be increased, however, by decreasing the active transducer area (decreasing C_0) even for small coupling, but at the expense of reduced bandwidth. Using high coupling transducers allows the radiating area to be increased while maintaining a wide bandwidth. Operating at the third harmonic allows a significantly larger transducer thickness (by approximately a factor of 3) for a given frequency, which also reduces C_0. The reduction in k_t^2, however, by a factor of 9 causes a degradation in the bandwidth, which more than compensates for the decreased capacitance.

Generally, transducers are operated at their fundamental resonance for best performance. Although not directly of concern here, for low frequency operation, $\hat{R}_a$ may be significantly *greater* than 50 Ω, which also prevents efficient energy conversion. Finally, increasing the radiating area for a given coupling constant has the effect of decreasing $\hat{R}_a$ and moving the characteristic clockwise around the chart, as shown in Figure 6.7. The clockwise rotation reflects the fact that X_C decreases as C_0 increases. The curves correspond to Example 6.1. For curve 1, $A = 3 \times 10^{-9}$ (50 Ω); for curve 2, $A = 6 \times 10^{-9}$; for curve 3, $A = 2 \times 10^{-8}$; and for curve 4, $A = 5 \times 10^{-8}$.

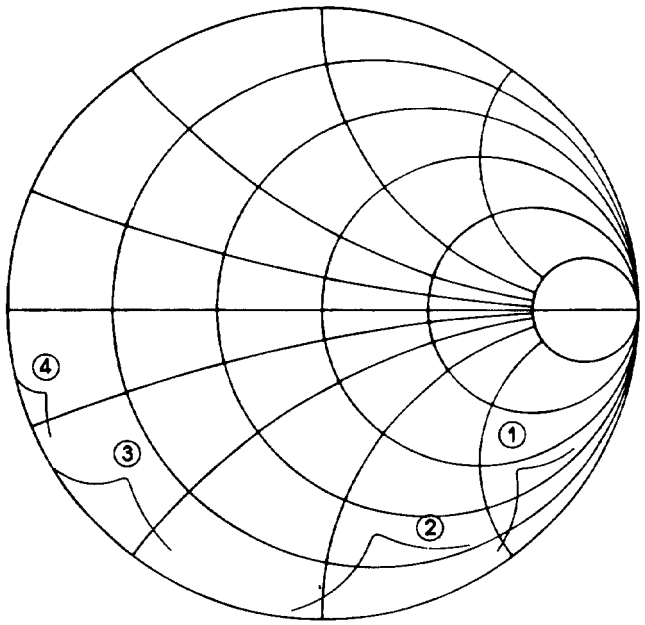

Figure 6.7 Effect of transducer area on the impedance characteristic. As the area increases, the characteristic moves clockwise around (C_0 increases) and toward the periphery of the chart (because R_a decreases).

Example 6.2. Discuss the impedance characteristic of Example 5.4 from its Smith chart plot. The previous example is characteristic of the case in which the transducer and substrate impedances are closely matched. A second example, characteristic of the case in which there is a large impedance mismatch between the transducer and substrate, is the important case of an ⟨*x*⟩ lithium niobate shear transducer rigidly bonded to the ⟨1, 1, 0⟩

face of paratellurite (TeO_2). Generally, the transducer will possess the higher impedance because there are many more important applications that require slow, low impedance acoustic modes (e.g., long delay lines and high resolution A/O spectrum analyzers) using relatively high impedance transducers than *vice versa*. In the present case, the transducer is oriented along the $\langle -1, 1, 0 \rangle$ direction of the substrate so as to excite the quasi (slow) shear mode (the weakly excited, orthogonally polarized shear mode is ignored). The relevant material constants are given in Example 5.4. The transducer thickness is approximately 40 μm, so the resonance occurs at approximately 50 MHz. Note that the transducer is much thicker than in the previous example, because the high acoustic attenuation (not considered in this model) of the slow shear mode seriously impairs device performance above 100 MHz.

Figure 6.8 shows the complex impedance and return loss for the foregoing conditions. From the Smith chart plot, it seems that the device is well matched. The RL plot, however, reveals that the match is over a very small fractional bandwidth. The bandwidth in this example is quite small, even though the coupling constant of the transducer is extremely high ($k_t^2 = .46$). The low bandwidth is due to the large impedance mismatch between the transducer and substrate. Also apparent from Figure 6.8 is that there is a large resonance "loop" causing the impedance to look inductive over an appreciable frequency range, in agreement with Figure 5.13. This is again a direct consequence of the large impedance mismatch. Because of this large mismatch, the acoustic energy transfer from the transducer to the substrate is not nearly as efficient as in the previous example. As the mismatch becomes larger (by using an even lower impedance substrate), the acoustic energy is increasingly confined to the transducer and the device looks more and more like a resonator. In the resonator structure, the substrate is replaced by air, which is an acoustic "short circuit" of zero impedance. In that case, all of the energy is confined to the transducer, resulting in an impedance "loop" that traverses the outer periphery of the Smith chart even if the transducer possesses a high coupling constant. Similar behavior would result if the transducer were bounded by very high impedances.

In contrast to the electrical case, where it is possible to produce a high-quality open, it is impossible to achieve an acoustic open circuit because the highest known impedance is only about three times larger than most typical transducer cuts. At any rate, efficient energy transfer over a wide band requires a close *acoustic* impedance match between substrate and transducer. Table 6.1 lists some practical transducer-substrate combinations and their typical applications. Notice that in most cases the transducer impedance is greater than the substrate impedance ($Z_S/Z_T < 1$). As mentioned previously, the substrate typically has significantly smaller impedance than the transducer does.

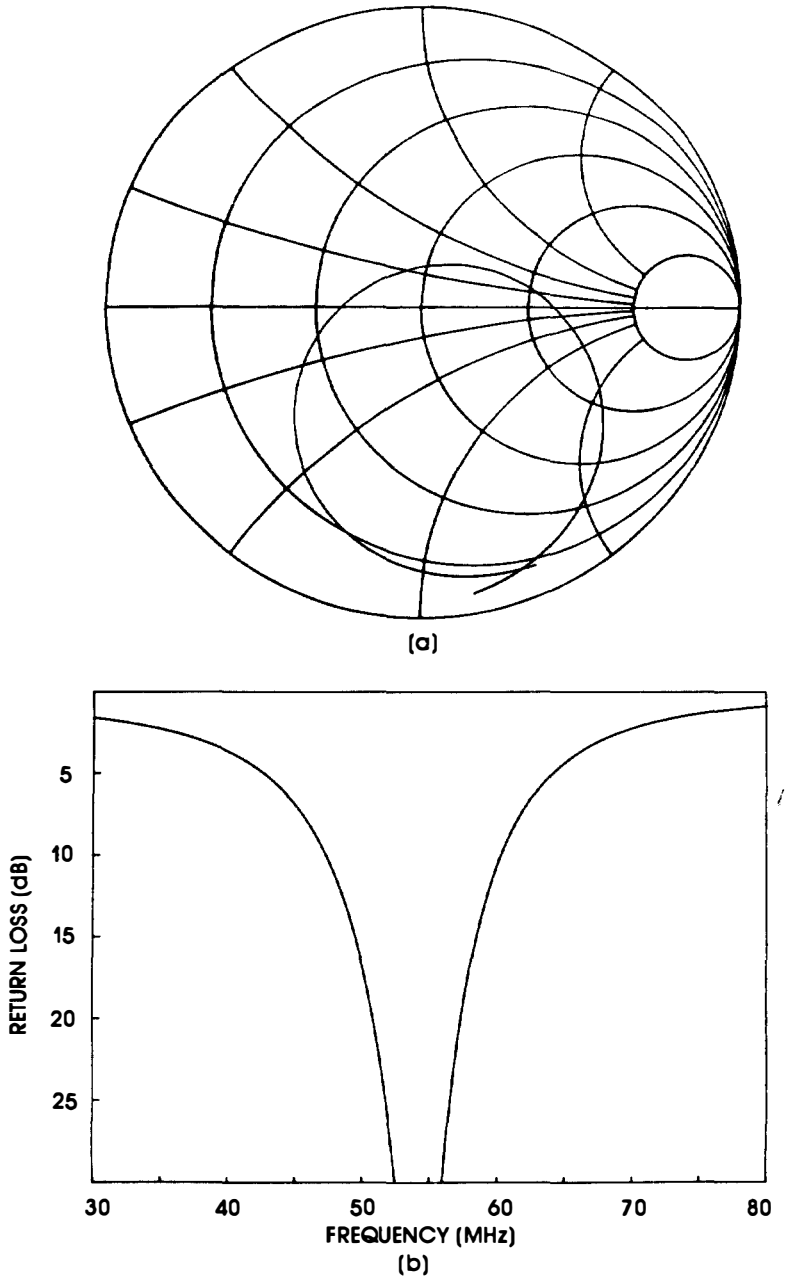

Figure 6.8 Impedance characteristic of TeO_2 with no bond layer. The transducer thickness is 40 μm, the area is $4 \times 10^{-6}\ m^2$, and the frequency range is from 30 to 80 MHz: (a) Smith chart plot; (b) return loss plot.

Table 6.1

Transducer	*Substrate*	Z_S/Z_T	*Application*
36° ⟨*y*⟩ $LiNbO_3$	⟨*x*⟩ $LiNbO_3$	.9	Wideband A/O deflector
36° ⟨*y*⟩ $LiNbO_3$	GaP ⟨1, 1, 0⟩ or ⟨1, 1, 1⟩	.8	Wideband A/O deflector
⟨*x*⟩ $LiNbO_3$	$MgAl_2O_3$	1.1	Delay line
36° ⟨*y*⟩ $LiNO_3$	⟨*z*⟩ TeO_2	.75	Wideband A/O deflector
36° ⟨*y*⟩ $LiNbO_3$	Ge ⟨1, 1, 0⟩ or ⟨1, 1, 1⟩	.85	10.6-μm A/O deflector
⟨*x*⟩ $LiNbO_3$	⟨1, 1, 0⟩ $Te0_2$	.2	High resolution A/O deflector
⟨*x*⟩ $LiNbO_3$	$HgCl_2$	<.2	High resolution A/O deflector

6.4 ONE-DIMENSIONAL MASON MODEL

6.4.1 Lumped Element Circuit Representation of Piezo- and Nonpiezo layers

The simple closed-form expressions of Chapter 5 provide valuable insight into the operation of acoustic devices, but do not accurately predict device performance, especially at high frequencies. A more realistic model of a wideband acoustic device can be constructed by using the full Mason model as developed in the previous chapter. The model includes multiple layers of piezoelectric and nonpiezoelectric layers of arbitrary thickness. It thus includes two important effects not considered in the simplified closed-form expressions of (5.53) and (5.54): the loading effects of metallic electrodes, and the possibility of standing acoustic waves the substrate. To fully account for these effects, we need to write the propagation constant in the substrate in complex form (see (1.18)). Routinely, attenuation is included in all layers, although its effect, in wideband operation, is usually minimal except in the substrate. Because the top electrode is usually aluminum, which has minimal loading effect, we usually do not require this element to be treated as an acoustic transmission line, but only as an impedance mismatch.

Manipulation of the acoustic and electroacoustic (piezoelectric) layers requires a representation in which it is possible to catenate multiple layers of various thicknesses and material properties together, as shown

in Figure 5.7. Consider, for example, the acoustic delay line lumped element circuit shown in Figure 5.2. In matrix form, we have

$$\begin{bmatrix} F_1 \\ F_2 \end{bmatrix} \rightarrow \begin{bmatrix} V_i \\ V_o \end{bmatrix} = \begin{bmatrix} a & b \\ b & a \end{bmatrix} \begin{bmatrix} I_i \\ -I_o \end{bmatrix} \tag{6.10}$$

where

$$\begin{bmatrix} I_i \\ I_o \end{bmatrix} \rightarrow \begin{bmatrix} v_2 \\ v_1 \end{bmatrix} \qquad a = \frac{Z}{j \sin(kd)} + jZ \tan\left(\frac{kd}{2}\right)$$

$$b = \frac{Z}{j \sin(kd)}$$

In (6.10), the forces and particle velocities are grouped together. A representation that permits the attachment of layers to either port requires that the input and output variables not be mixed, as in (6.10). We manipulate the acoustic equations so that

$$\begin{bmatrix} V_o \\ I_o \end{bmatrix} = \begin{bmatrix} A & B \\ C & D \end{bmatrix} \begin{bmatrix} V_i \\ I_i \end{bmatrix} \tag{6.11}$$

In (6.11), the acoustic output variables, "voltage" (force) and "current" (particle velocity), are written in terms of the input variables. The output variables of a particular acoustic layer become the input variables of the acoustic layer neighboring on the right. Written in this manner, the material constants resemble *ABCD* parameters [6]. From the definition of the *ABCD* parameters,

$$\begin{aligned} A &= \left.\frac{V_o}{V_i}\right|_{I_i=0}, \quad B = \left.\frac{V_o}{I_i}\right|_{V_i=0} \\ C &= \left.\frac{I_o}{V_i}\right|_{I_i=0}, \quad D = \left.\frac{I_o}{I_i}\right|_{V_i=0} \end{aligned} \tag{6.12}$$

To determine A, we need $I_i = 0$; that is, the particle velocity is zero at the left boundary (the left side is rigidly clamped). Referring to the circuit in Figure 6.9, we see that the output becomes a simple voltage divider, so (using standard trigonometric identities)

$$A = \cos(kd), \quad B = -jz \sin(kd) \tag{6.13}$$

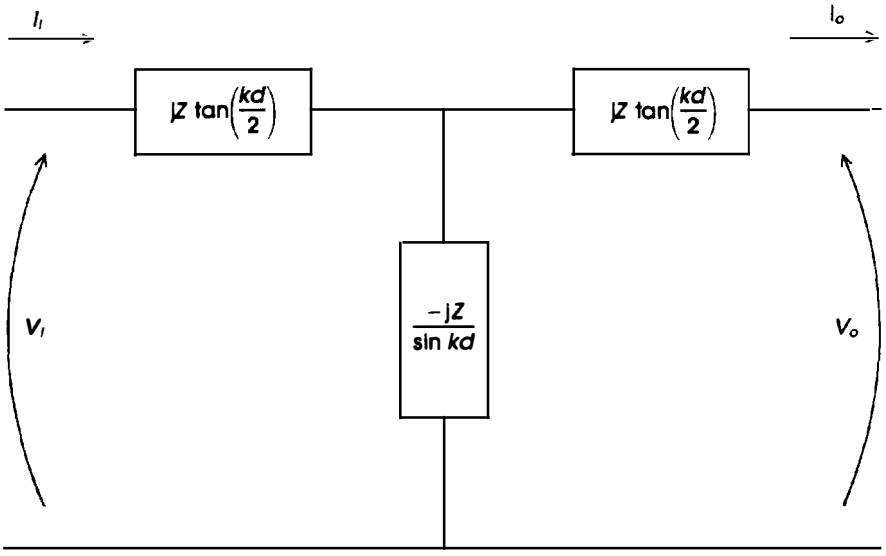

Figure 6.9 Model of an acoustic transmission line showing input variables I_i (particle displacement) and V_i (force) and output variables I_o and V_o.

Similarly, by requiring $V_i = 0$, which is the stress-free condition at the left boundary, we can easily show that

$$C = -j\frac{\sin(kd)}{Z}, \quad D = A = \cos(kd) \tag{6.14}$$

Substituting these values into (6.11), we have

$$\begin{vmatrix} A & B \\ C & D \end{vmatrix} = 1$$

Attenuation can be easily injected into this formulation by requiring the propagation constant k to be complex. The $ABCD$ parameters become complex, and we have

$$\begin{aligned} \hat{A} &= \cos(\hat{k}d) = \cosh(\alpha d)\cos(kd) - j\sinh(\alpha d)\sin(kd) = \hat{D} \\ \hat{B} &= -Z\,(\sinh(\alpha d)\cos(kd) + j\cosh(\alpha d)\sin(kd) \\ \hat{C} &= -\frac{1}{2}\,(\sinh(\alpha d)\cos(kd) + j\cosh(\alpha d)\sin(kd)) \end{aligned} \tag{6.15}$$

where the circumflex represents a complex number. Equations (6.15) reduce to (6.13) and (6.14) as $\alpha \rightarrow 0$.

The circuit representation of the piezoelectric layer follows a similar procedure. The representation is somewhat more complex because it is a three-port, mixed electrical-acoustic circuit. A significant simplification occurs if the acoustic input port is stress-free ($F_1 = 0$). In this case, the acoustic input port is shorted so that Figure 5.6 reduces to a two-port circuit as shown in Figure 6.10. This representation corresponds to the case in which the transducer looks into air. In practice, the input acoustic port must be plated with a thin (usually only about .1 μm) electrode, usually aluminum; it is best to replace the short with an acoustic impedance (Z_1) between terminals 1 and 2. It can be shown that this representation (in which the top electrode is replaced by an impedance) is valid even at very high frequencies. If a thicker backing material or gold is required as the top electrode, it may be necessary to replace this element with a lossy acoustic delay line, which complicates the circuit. The circuit in Figure 6.10 is similar to that of Figure 6.9 except that the input variables are electrical and the output variables are acoustic. The parameters A and C are determined by requiring that $I_i = 0$ (electrical input current). With this condition, Figure 6.10 is transformed into the circuit of Figure 6.11 by using standard circuit techniques to eliminate the transformer. Writing Kirchhoff's voltage laws for loops 1 and 2, we find that (assuming a short circuit at terminals 1 and 2):

$$A = \frac{j\omega C_0(a^2 + 2ab)}{\phi a}$$
$$C = \frac{-j\omega C_0(a + b)}{\phi a} \tag{6.16}$$

where $a = jZ \tan(kd/2)$ and $b = -jZ/\sin(kd)$.

Similarly, by requiring that the electric voltage V_i be zero, we can show that

$$B = -\frac{2ja\phi^2/\omega C_0 + (a^2 + 2ab)}{\phi a}$$
$$D = \frac{j\phi^2/\omega C_0 + a + b}{\phi a} \tag{6.17}$$

Equations (6.16) and (6.17) assume that the transducer looks into air. If the impedance of the top electrode is included, the equations are slightly more involved. As in the acoustic delay line, attenuation is introduced by allowing the propagation constant to be complex.

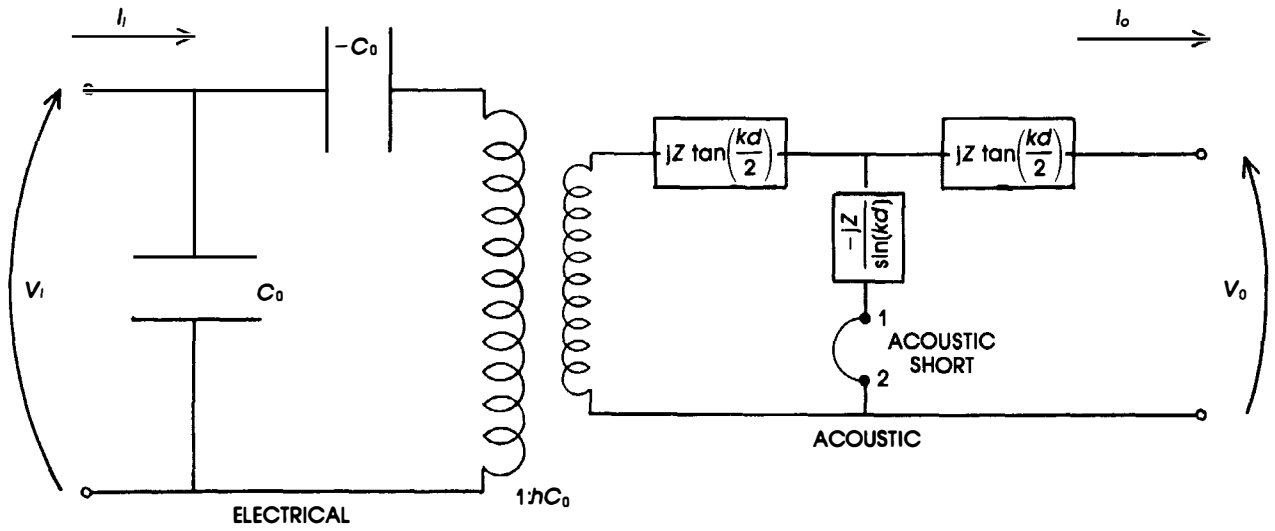

Figure 6.10 Mason model of a piezoelectric layer showing the shorted acoustic port, which dramatically simplifies computations.

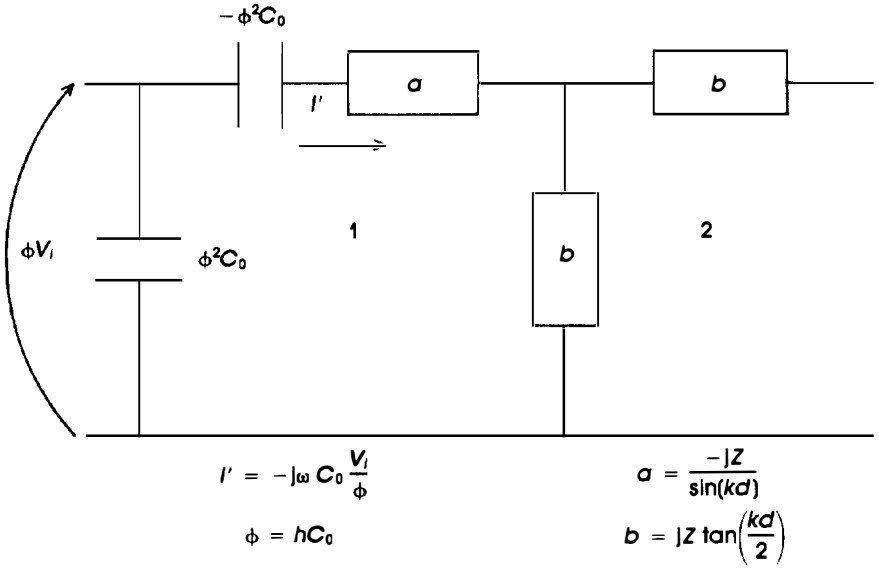

Figure 6.11 Circuit representation of piezoelectric layer for computation of *ABCD* parameters.

6.4.2 Computer-Aided Analysis of Acoustic Devices

Figure 6.12 is a computer program that uses these principles to calculate the input impedance of an acoustic device. The program calculates the input impedance of a device with one transducer, a top electrode (which is treated as an impedance), a metallic ground plane, and a substrate. It includes the effects of attenuation in all (four) layers, metallic loading effects, and a finite-length substrate. It can easily be modified to include two transducers and more acoustic delay elements. It is divided into a number of distinct components:

1. Lines 1180 to 1570 draw the Smith chart circles of constant resistance and reactance. The centers and radii of these circles are given by (6.5) and (6.6).

2. Lines 1660 to 2350 input the data, which include the radiating area, and the impedance, velocity, thickness, and attenuation of each layer. The attenuation is input as a vector because it changes with frequency; the data values correspond to the attenuation in Np/m at 1 GHz. In line 2620, we calculate the attenuation at the required frequency by assuming an f^2 dependence (perfect crystal structure). The first letter in each data line corresponds to the element (*T* for top electrode, *P* for piezolayer), and the second letter corresponds to the parameter (*I* for impedance, *et cetera*).

```
1000  !THIS PROGRAM COMPUTES THE INPUT IMPEDANCE OF AN ACOUSTIC DEVICE
1030  LIBRARY "GRAPHLIB" !INTERNAL LIBRARY FUNCTIONS
1060  SET MODE "HIRES"  !SETS THE GRAPHICS MODE
1090  LIBRARY "ARC"
1120  SET WINDOW -1.3,1.3,-1,1
1150  !THIS ROUTINE DRAWS THE SMITH CHART CIRCLES
1180  BOX CIRCLE -1,1,-1,1
1210  BOX CIRCLE 0,1,-.5,.5
1240  DRAW BOXARC(-9,11,0,20,258.6,270)
1270  DRAW BOXARC(-9,11,-20,0,90,101.4)
1300  BOX CIRCLE -.3,1,-.65,.65
1330  PLOT -1,0;1,0
1360  BOX CIRCLE .3,1,-.35,.35
1390  BOX CIRCLE -.75,1,-.875,.875
1420  DRAW BOXARC (0,2,0,2,180,270)
1450  DRAW BOXARC(0,2,-2,0,90,180)
1480  DRAW BOXARC(.5,1.5,0,1,145,270)
1510  DRAW BOXARC(.5,1.5,-1,0,90,218)
1540  DRAW BOXARC(-1,3,0,4,217,270)
1570  DRAW BOXARC(-1,3,-4,0,90,143)
1600  DIM A1(4),B1(4)
1630  !LINES 1660 TO 2350 INPUT THE DATA
1660  LET AA=8.8E-08  !RADIATING AREA OF TRANSDUCER
1690  !TOP ELECTRODE; VALUES ARE FOR ALUMINUM
1720  LET TI=1.72E+07*AA  !TOP ELECTRODE ACOUSTIC IMPEDANCE
1750  LET TV=6350  !TOP ELECTRODE ACOUSTIC VELOCITY
1780  LET TT=1E-7  !TOP ELECTRODE THICKNESS
1810  LET A1(1)=236.2  !ATTENUATION OF ELECTRODE AT 1 GHz
1840  !PIEZOLAYER; VALUES ARE FOR LITHIUM NIOBATE 36 <Y>
1870  LET PI1=3.3E+7*AA
1900  LET PV=7400
1930  LET PT=2.5E-6
1960  LET A1(2)=1.5
1990  !GROUND PLANE; VALUES ARE FOR GOLD
2020  LET GI=6.56E+07*AA
2050  LET GV=3400
2080  LET GT=5E-7
2110  LET A1(3)=1924
2140  !SUBSTRATE; VALUES ARE FOR GALLIUM PHOSPHIDE <1,1,0>
2170  LET SI= 3.4E+07*AA
2200  LET SV=6500
2230  LET ST=.1
2260  LET A1(4)=150
2290  LET EE=3.45E-10 !PERMITTIVITY OF LITHIUM NIOBATE 36 <Y>
2320  LET C0=AA*EE/PT  !CLAMPED CAPACITANCE C0
2350  LET K2=.25  !COUPLING CONSTANT SQUARED
2380  INPUT PROMPT "START FREQUENCY": Q
2410  INPUT PROMPT "STOP FREQUENCY":  R
2440  INPUT PROMPT "NUMBER OF POINTS": T
2470  LET QF=R
2500  LET R=(R-Q)/T
2530  LET T=T+1
2560  FOR S=1 TO T !THIS IS THE MAIN LOOP
2590  FOR M=1 TO 4
2620  LET B1(M)=A1(M)*(Q*1E-09)^2 !FREQUENCY SQUARED DEPENDENCE OF ATTENUATION
2650  NEXT M
2680  LET W=2*PI*Q
2710  !DELAY PROGRAM FOR SUBSTRATE
2740  LET T1=EXP(B1(4)*ST)
2770  LET T2=1/T1
```

Figure 6.12 Computer listing of program to calculate the impedance characteristic of acoustic device with four layers of arbitrary thicknesses and acoustic properties.

```
2800  LET T3=(T1+T2)/2
2830  LET T4=(T1-T2)/2
2860  LET T5=COS(W*ST/SV)
2890  LET T6=SIN(W*ST/SV)
2920  LET G=T3*T5
2950  LET A=G
2980  LET H=T4*T6
3010  LET B=H
3040  LET C=T4*T5
3070  LET E=-C/SI
3100  LET C=-C*SI
3130  LET D=T3*T6
3160  LET F=-D/SI
3190  LET D=-D*SI
3220  !DELAY PROGRAM FOR GROUND PLANE
3250  LET T1=EXP(B1(3)*GT)
3280  LET T2=1/T1
3310  LET T3=(T1+T2)/2
3340  LET T4=(T1-T2)/2
3370  LET T5=COS(W*GT/GV)
3400  LET T6=SIN(W*GT/GV)
3430  LET O=T3*T5
3460  LET I=O
3490  LET P=T4*T6
3520  LET J=P
3550  LET K=T4*T5
3580  LET M=-K/GI
3610  LET K=-K*GI
3640  LET L=T3*T6
3670  LET N=-L/GI
3700  LET L=-L*GI
3730  !MATRIX MULTIPLICATION
3760  LET T1=A*I-B*J+C*M-D*N
3790  LET T2=A*J+B*I+C*N-D*M
3820  LET T3=A*K-B*L+C*O-D*P
3850  LET T4=B*K+A*L+C*P+D*O
3880  LET T5=E*I-F*J+G*M-H*N
3910  LET T6=E*J+F*I+G*N+H*M
3940  LET T7=E*K-F*L+G*O-H*P
3970  LET T8=E*L+F*K+G*P+H*O
4000  LET A=T1
4030  LET B=T2
4060  LET C=T3
4090  LET D=T4
4120  LET E=T5
4150  LET F=T6
4180  LET G=T7
4210  LET H=T8
4240  !IMPEDANCE OF TOP ELECTRODE
4270  LET T1=EXP(B1(1)*TT)
4300  LET T2=1/T1
4330  LET T3=(T1+T2)/2
4360  LET T4=(T1-T2)/2
4390  LET T5=COS(W*TT/TV)
4420  LET T6=SIN(W*TT/TV)
4450  LET T7=TI*T4/(T3+T5)
4480  LET T8=TI*T6/(T3+T5)
4510  LET T9=T4*T5/TI
4540  LET T10=T3*T6/TI
4570  LET T11=T7
```

```
4600  LET T12=T8
4630  LET T13=T11*T11+T12*T12
4660  LET T11=T11/T13
4690  LET T12=T12/T13
4720  LET T11=T11+T9
4750  LET T12=T12+T10
4780  LET T14=T11*T11+T12*T12
4810  LET T11=T11/T14
4840  LET T12=T12/T14
4870  LET R1=T11+T7
4900  LET R2=T12+T8
4930  !MASON MODEL FOR PIEZOELECTRIC LAYER
4960  LET T1=PI1*PV*C0*K2/(PT*(1+K2))
4990  LET T2=SQR(T1)
5020  LET T3=EXP(B1(2)*PT)
5050  LET T4=1/T3
5080  LET T5=(T3+T4)/2
5110  LET T6=(T3-T4)/2
5140  LET T7=COS(W*PT/PV)
5170  LET T8=SIN(W*PT/PV)
5200  LET T9=PI1*T6/(T5+T7)
5230  LET T10=T9
5260  LET T11=T9
5290  LET T12=PI1*T8/(T5+T7)
5320  LET T13=T12
5350  LET T14=T12
5380  LET T15=T6*T7/PI1
5410  LET T16=T5*T8/PI1
5440  LET T17=T15*T15+T16*T16
5470  LET T18=T15/T17
5500  LET T19=-T16/T17
5530  LET T7=T9
5560  LET T8=T12
5590  LET T7=T7+R1
5620  LET T8=T8+R2
5650  LET T7=T2*T7
5680  LET T8=T2*T8
5710  LET T20=T7*T7+T8*T8
5740  LET T7=T7/T20
5770  LET T8=-T8/T20
5800  LET T21=T10*T9-T13*T12
5830  LET T13=T10*T12+T13*T9
5860  LET T10=T21
5890  LET T22=T11*R1-T14*R2
5920  LET T14=T11*R2+T14*R1
5950  LET T11=T22
5980  LET T10=T10+T11
6010  LET T13=T13+T14
6040  LET T11=T18
6070  LET T14=T19
6100  LET T23=T11*R1-T14*R2
6130  LET T14=T11*R2+T14*R1
6160  LET T11=T23
6190  LET T10=T10+T11
6220  LET T13=T13+T14
6250  LET T11=2*T9
6280  LET T14=2*T12
6310  LET T24=T11*T18-T14*T19
6340  LET T14=T11*T19+T14*T18
6370  LET T11=T24
```

```
6400  LET T10=T10+T11
6430  LET T13=T13+T14
6460  LET I=T13*W*C0
6490  LET J=-T10*W*C0
6520  LET T25=I*T7-J*T8
6550  LET J=I*T8+T7*J
6580  LET I=T25
6610  LET T11=2*T9
6640  LET T14=2*T12
6670  LET T11=T11+R1
6700  LET T14=T14+R2
6730  LET K=-T1*T14/W/C0
6760  LET L=T1*T11/C0/W
6790  LET K=K+T10
6820  LET L=L+T13
6850  LET T26=K*T7-L*T8
6880  LET L=K*T8+L*T7
6910  LET K=T26
6940  LET T10=T18
6970  LET T13=T19
7000  LET T10=T10+T9
7030  LET T13=T13+T12
7060  LET T10=T10+R1
7090  LET T13=T13+R2
7120  LET M=-T13*C0*W
7150  LET N=T10*C0*W
7180  LET T27=M*T7-N*T8
7210  LET N=M*T8+N*T7
7240  LET M=T27
7270  LET O=-T10
7300  LET P=T13+T1/C0/W
7330  LET P=-P
7360  LET T28=O*T7-P*T8
7390  LET P=O*T8+P*T7
7420  LET O=T28
7450  !MATRIX MULTIPLICATION OF PIEZOLAYER WITH GROUND PLANE
7480  LET T1=A*I-B*J+C*M-D*N
7510  LET T2=A*J+B*I+C*N-D*M
7540  LET T3=A*K-B*L+C*O-D*P
7570  LET T4=B*K+A*L+C*P+D*O
7600  LET T5=E*I-F*J+G*M-H*N
7630  LET T6=E*J+F*I+G*N+H*M
7660  LET T7=E*K-F*L+G*O-H*P
7690  LET T8=E*L+F*K+G*P+H*O
7720  LET A=T1
7750  LET B=T2
7780  LET C=T3
7810  LET D=T4
7840  LET E=T5
7870  LET F=T6
7900  LET G=T7
7930  LET H=T8
7960  LET A2=A*A+B*B !CONVERSION OF IMPEDANCE TO SMITH CHART COORDINATES
7990  LET A=A/A2
8020  LET B=-B/A2
8050  LET A3=C*A-D*B
8080  LET D=C*B+D*A
8110  LET C=A3
8140  LET G=C
8170  LET H=D
```

```
 8200  LET G=-G
 8230  LET H=-H
 8260  LET M=G
 8290  LET N=H
 8320  LET E=G-50
 8350  LET F=H
 8380  LET G=G+50
 8410  LET A4=G*G+H*H
 8440  LET G=G/A4
 8470  LET H=-H/A4
 8500  LET A5=E*G-F*H
 8530  LET F=E*H+F*G
 8560  LET E=A5
 8590  !PRINT E,F
 8620  PLOT E,F; !E AND F ARE NORMALIZED TO 50 OHMS
 8650  LET  Q=Q+R
 8680  NEXT S
 8710  END
```

In addition, the dielectric constant and k_t^2 are required for the piezolayer. The velocities and coupling constant are determined from the Christoffel equation.

3. The substrate and ground plane are treated as acoustic delay lines and are described by matrices of the form of (6.10). The composite structure, consisting of the *ABCD*-parameters of both delay lines is described by the product of the two separate lines, as shown in lines 3760 to 4210.

4. The piezolayer matrix (including the top electrode) is determined from the circuit of Figure 6.10; it is catenated onto the substrate ground plane by multiplying its matrix with the *ABCD*-parameter matrix of the composite substrate ground structure to arrive at an *ABCD* parameter matrix that completely describes the device. The input impedance depends on the acoustic properties of all layers and on the frequency.

5. Finally, the impedance is converted to Smith chart coordinates in lines 7960 to 8560 (i.e., reflection coefficient) and plotted. The return loss is plotted by using (6.7).

6.5 EFFECT OF GROUND PLANE METALIZATION

Results for the configuration of Example 6.1, in which an aluminum top electrode and gold ground plane of .2 μm have been added, are shown in Figure 6.13. Gold is usually used as the ground electrode when the transducer is vacuum welded to the substrate, although silver, aluminum, tin, and indium are also common. Two differences between the closed-form characteristic and the Mason model are immediately apparent:

1. The resonance frequency has been dramatically reduced.
2. The impedance characteristic has formed a loop around the center frequency.

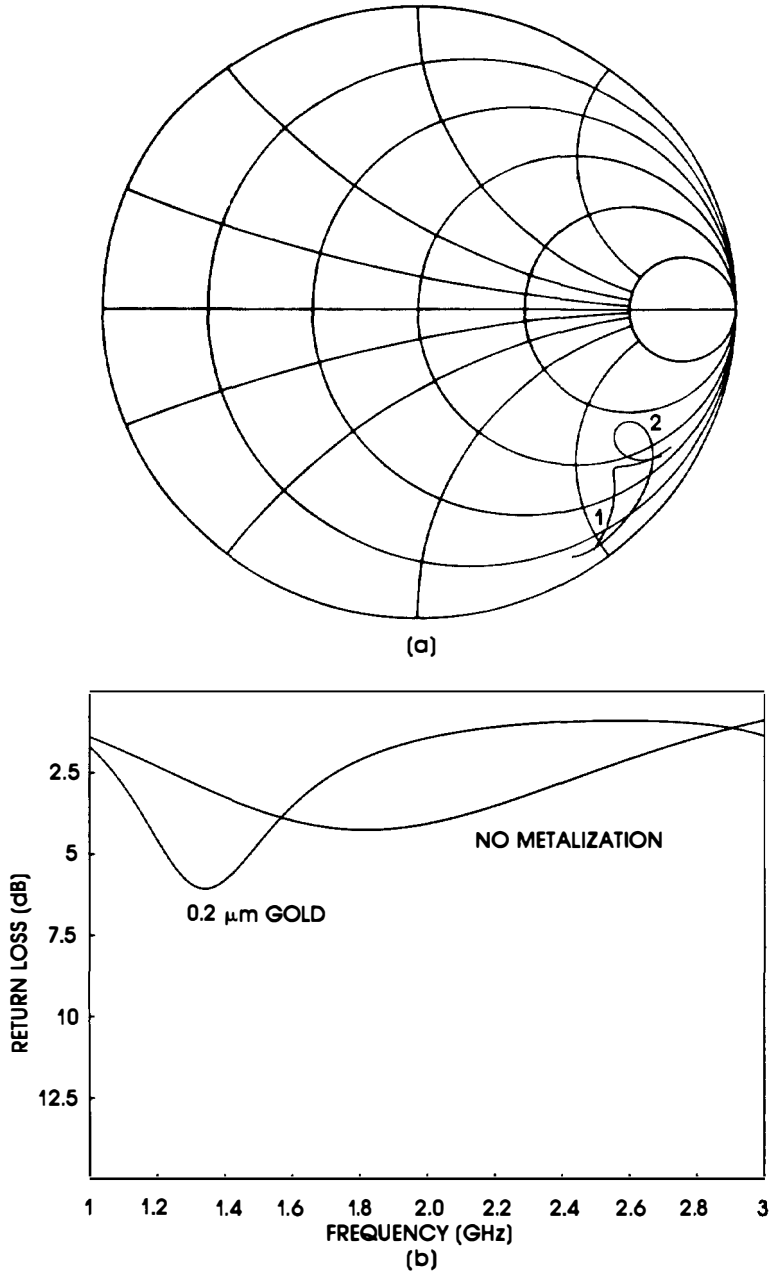

Figure 6.13 Input impedance of longitudinal mode lithium niobate transducer on ⟨x⟩ lithium niobate substrate showing the effect of gold ground plane metalization. Parameters are identical to Figure 6.5: curve 1; no metalization; curve 2; .2 μm gold metalization.

The ground electrode reduces the resonance frequency by its presence as part of the acoustic path of the transducer. We say that it acoustically "loads" the transducer. The effect is significantly more pronounced with gold because of its low acoustic velocity. The resonant frequency no longer occurs at the halfwave resonance of the transducer. At 2 GHz, there is very little acoustic energy introduced into the substrate, as indicated by the small return loss. Indeed, it is difficult to get an accurate quantitative measure for the frequency reduction due to acoustic mass loading without actually modeling the complete multilayered system. Generally, however, it is correct to state that at low frequencies the large transducer thickness permits much greater metalizations with little or no loading, but above 1 GHz the ground metalization must be considered as a first-order effect. For instance, in the present example the frequency reduction is over 25%. The effect is more significant when shear wave transducers are used, due to their lower acoustic velocities, so even a thin ground plane is significant.

The impedance loop in Figure 6.13(a) is due to the severe acoustic mismatch between the transducer and substrate. The electrode effectively looks like a substrate with impedance (in the case of gold) twice that of the transducer. Unfortunately, gold is severely mismatched to nearly all transducer materials; its high impedance is due to its high density. We can show, using the computer model, that for a given electrode thickness the size of the loop increases for large coupling constant and decreases for small k_t^2 (measuring the size of the loop is a convenient test of the coupling constant). Later, we will show that proper choice of the acoustic properties and thickness of the ground plane can actually increase the bandwidth in cases in which the transducer and substrate are severely mismatched, as in example 6.2. Table 6.2 lists the properties of some popular ground electrode metals. Because the ground plane is always extremely thin compared with the substrate, its attenuation is usually not very important, except when gold is used at frequencies above 5 GHz in the shear mode or indium is used at frequencies above 1 GHz.

Compared with other metals, the larger impedance and lower velocity of gold tend to degrade the high frequency operation more than other choices of ground metalizations. This is illustrated in Figure 6.14, which shows the return loss of a lithium niobate-lithium niobate device with a gold ground plane thickness of 5000 Å. In order to return the resonant frequency of the device to about 1.6 GHz (the resonant frequency with .2 μm gold), we must reduce the transducer thickness to 1 μm. Under these conditions, in which the gold constitutes nearly half of the transducer

Table 6.2 (*Note*: all units are MKS)

Metal	*Velocity (km/sec)*	*Density* $(kg/m^3) \times 10^3$	*Impedance*	*Attenuation (N/m)*
Au (long.)	3.2	19	66×10^6	1900
Au (shear)	1.47	19	34	>2500
Al (long.)	6.35	1.7	17	240
Al (shear)	3.3	1.7	8.8	
Ag (long.)	3.44	10	34	2600
Ag (shear)	2.1	10	21	
In (long.)	2.5	7.2	18	>3000
In (shear)	1.3	7.2	9.4	

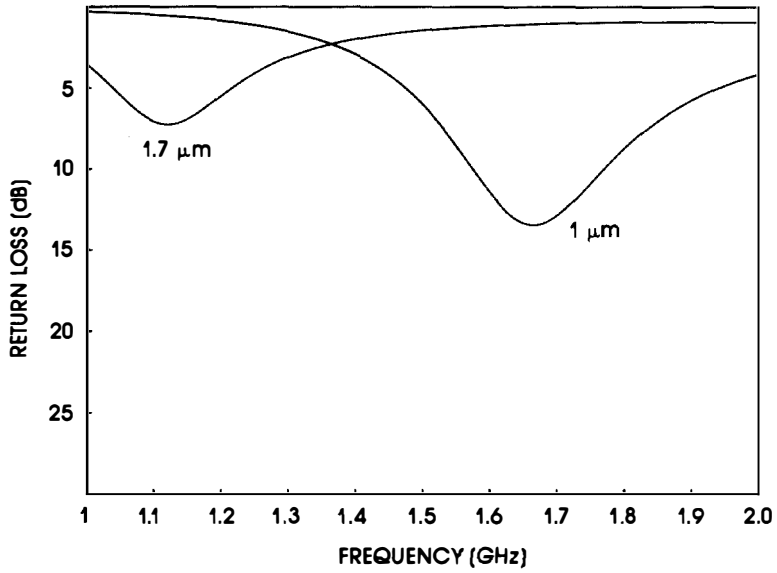

Figure 6.14 Return loss of device in Figure 6.13 when the gold layer has been increased to .5 μm. The transducer thickness must be reduced to 1 μm to achieve a resonance peak at about 1.6 GHz.

resonating structure, reducing the transducer thickness further would not appreciably increase the resonant frequency. The resonance is determined to a large degree by the ground plane thickness. It is not difficult to appreciate the severe impact of thick gold metalizations at very high frequencies. Additionally, the resonance loop will generally be larger, with thicker gold causing a good match only over a narrow bandwidth. Using aluminum or silver ground planes would significantly reduce loading effects. As we see from Table 6.2, silver is closely matched to lithium niobate and thus shows relatively little loading effects. Using silver, for example, results in a Smith chart impedance that resembles the curve of Figure 6.5 without the loop of Figure 6.13(a). Using aluminum actually causes an increase in the resonant frequency, but at the expense of a dramatically reduced bandwith. This occurs because the impedance of aluminum is much less than that of lithium niobate, so aluminum resembles a low impedance substrate with the resulting reduction in bandwidth (compare Figure 5.10 (a)). Because of the severe impedance mismatch, there is also a large loop in the impedance characteristic with aluminum ground planes.

Using gold has an interesting and potentially useful consequence not applicable in aluminum or silver metalizations. Its higher impedance causes an extra resonance that is not present when other metalizations are used. The presence of this resonance is consistent with Figure 5.10(b), which shows that the real part of the acoustic contribution to Z_{in} exhibits a double-humped characteristic for $Z_S/Z_T > 1$. Although the gold metalization is certainly not thick enough to qualify as a substrate, it shows the same behavior. Figure 6.15 shows the computer model of a fabricated A/O device consisting of 36° ⟨y⟩ $LiNbO_3$ on ⟨1, 1, 1⟩ GaP with a .5-μm gold ground plane. The area is 1×10^{-8} m^2. This particular configuration is quite important in a wideband spectrum analysis and will be studied more fully in Chapter 8. This device was designed to operate at 1 GHz, which requires a transducer thickness of about 2.5 μm. The loading effect of the gold was significantly less than in Example 6.1 (about 15%), due to the lower frequencies. Agreement of the model with measured results was excellent. The gold resonance loop that occurs at about 2 GHz was observed and used to increase the acoustic bandwidth of the device. The strength and frequency location of these extra resonances require computer modeling, but they are sufficiently strong to allow significant energy conversion. The chief disadvantage of all metals besides gold is that they will eventually oxidize, thus causing reliability problems in the integrity of the bond.

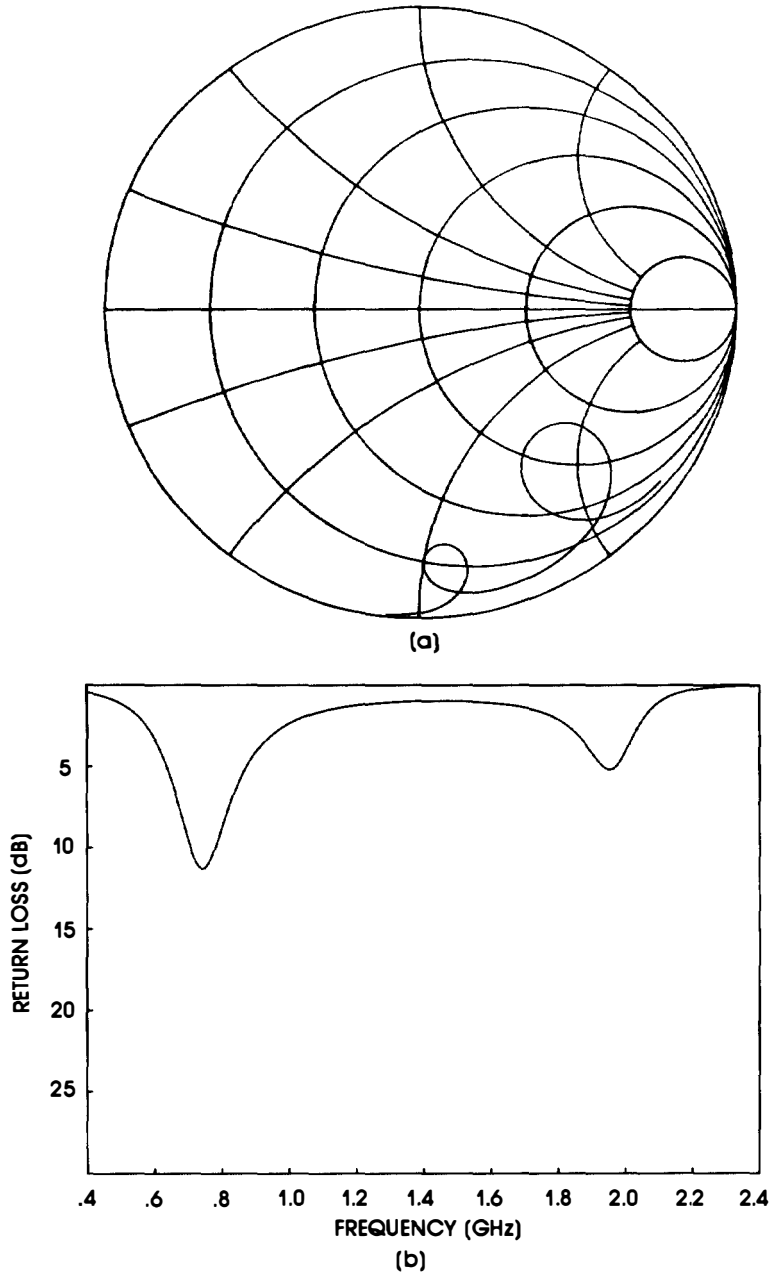

Figure 6.15 Input impedance of longitudinal lithium niobate on gallium phosphide ((1, 1, 1)) with .5 μm gold ground. Note the gold resonance peak near 2 GHz.

6.6 EFFECT OF FINITE SUBSTRATE LENGTH

The second important phenomenon included in the one-dimensional Mason model is the effect of a finite-length substrate. Physically, it is clear that if the far end of the substrate in a single transducer device is polished and parallel to the transducer face, the acoustic wave will be reflected back to the transducer, creating an acoustic standing wave. Because the reflected wave will be partially converted from acoustic energy to electrical energy, the presence of the standing waves may dramatically affect the impedance characteristic. In this configuration, the substrate is acting as an acoustic Fabry-Perot interferometer. The frequency separation between the maxima of the standing waves is

$$\Delta f = \frac{v_a}{2L} \tag{6.18}$$

for the propagating mode, where L is the length and v_a is the acoustic phase velocity of the substrate. The complex impedance characteristic for a finite length acoustic substrate is shown in Figure 6.16. The effect of the standing waves is to modulate the input impedance and, thus, the reflection coefficient, so the electrical power converted into acoustic power is a very sharp periodic function of frequency. The characteristic corresponds to Example 6.1 with a .5-μm gold ground. The frequencies of the loops are given by (6.18); the number of loops in a given frequency band increases linearly with substrate length. Also, at higher frequencies the loops decrease in size due to the frequency squared dependence of the attenuation. Such behavior is unacceptable in most A/O applications because the deflected light would be modulated in intensity at the standing wave frequency Δf. Likewise, in an acoustic delay line application (in which the reflections are referred to as triple transits), the insertion loss would be modulated in the same fashion. In an A/O deflector, it is customary either to roughen the far end of the substrate so as to disperse the acoustic wave or to cut it at an angle so as to deflect the wave harmlessly away from the laser. In delay line devices, the substrate is chosen to have a high enough attenuation so that the standing waves are effectively suppressed. We note that if the attenuation is low enough, the loops could increase in size sufficiently so that the characteristic will become inductive. If the attenuation in the substrate is very low, the resonances can have extremely high Q, which is exploited in a device called a high overtone bulk acoustic resonator (HBAR). We will look into HBAR design in more detail in Chapter 11.

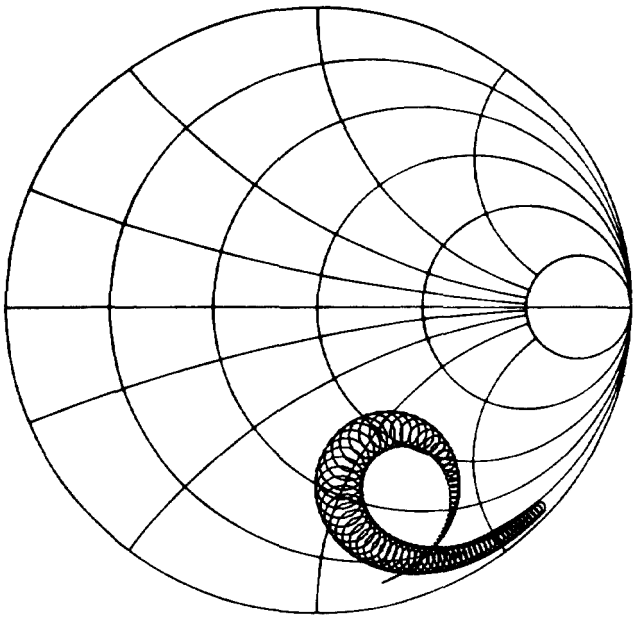

Figure 6.16 Finite substrate length modulates the impedance characteristic, causing resonance loops at the Fabry-Perot frequencies.

6.7 EXTERNAL TUNING ELEMENTS

6.7.1 Series Inductor

It is clear from the Smith chart curves that if standing wave effects can be neglected and the impedance mismatch is not too large, the impedance characteristic is capacitive at all frequencies. Practical devices, however, are electrically connected to transmission lines with bond wire, which has about 2 nH per 100 mil for a .7-mil-diameter gold or aluminum wire (the exact value depends on the position of the wire with respect to ground). At very high frequencies, this series inductance may cause the overall characteristic to look inductive.

A typical characteristic is shown in Figure 6.17 with and without a bond wire. By choosing the length and diameter of the bond wire carefully, we can, in principle, cancel the capacitive reactance of C_0 at *resonance*, thus resulting in a reflection coefficient of zero. The value of the required inductor depends on C_0, which is determined by the transducer area and

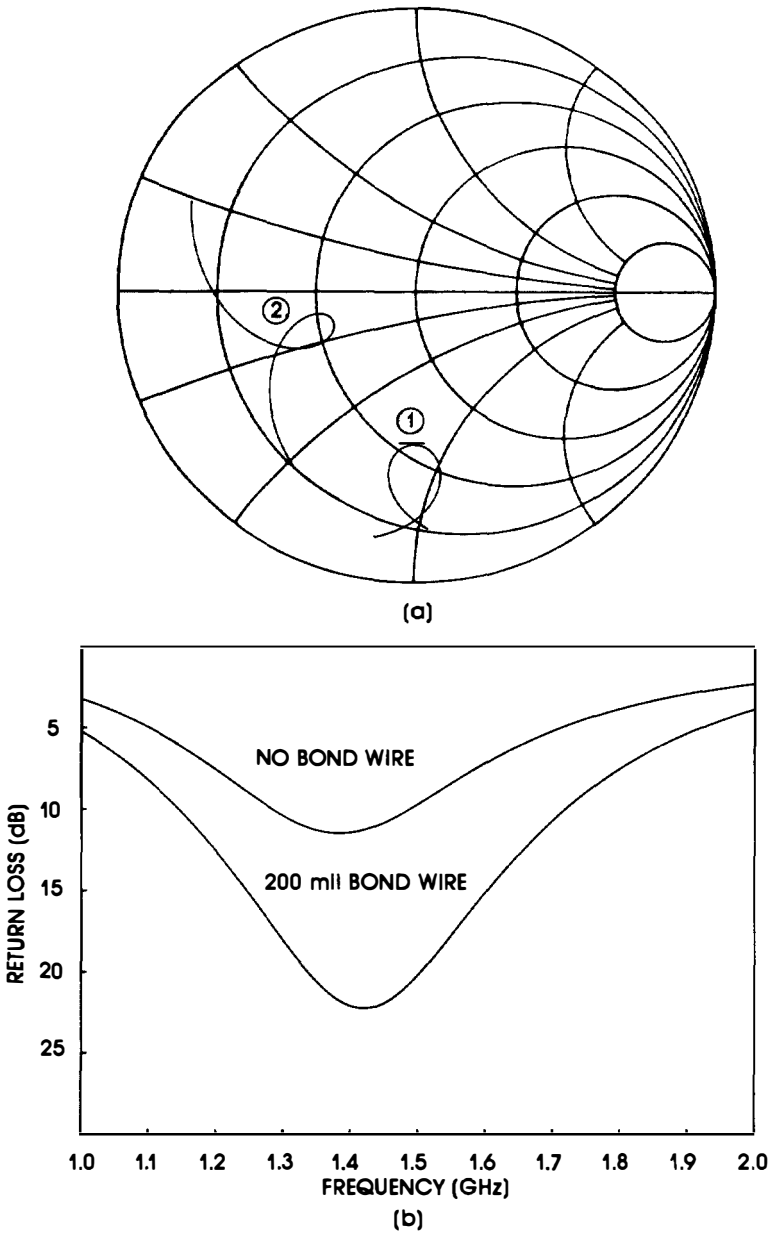

Figure 6.17 The effect of a series inductance is to move the characteristic along circles of constant reactance: curve 1; the characteristic with no external element; curve 2; the same device with a series bond wire of 200 mils. Note how the characteristic has spread. The parameters are those of Figure 6.13 with $A = 1 \times 10^{-8}$ m^2.

the piezoelectric dielectric constant. To cancel the capacitive reactance, however, we must carefully control bond wire length and make sure that the radiation resistance is precisely 50 Ω, which severely restricts the transducer dimensions, especially at high frequency operation. Long bond wire may be quite resistive and cause a decrease in the power introduced into the transducer. Furthermore, a series inductance generally has the effect of "spreading" out the impedance characteristic, as shown in Figure 6.17. Thus, unless the area can be chosen so that the radiation resistance is 50 Ω, it is usually good practice to keep the bond wires as short as possible. The addition of external tuning elements (usually parallel capacitors and inductors) is an extremely important consideration in the optimization of device performance. The effect of a series inductor on a typical impedance characteristic is shown in Figure 6.18 for a lithium niobate longitudinal transducer on ⟨1, 1, 1⟩ GaP with a 5-Å gold ground layer. It is a clear from this figure that the addition of the series inductance significantly improved the power conversion, even though the characteristic shows significant spreading. The required inductance (at the resonant frequency of 1 GHz) is larger than could be supplied by a bond wire, however. In this model, the inductor does not have a resistance associated with it. High-quality, low resistance inductors are available only at frequencies below 1 GHz, and thus the technique usually works best for lower frequencies. The ability of the inductance to "tune" out C_0 requires that the untuned characteristic be located near the $r = 1$ circle. If the characteristic had been located in a different position in the Smith chart, a series inductor could conceivably harm the device performance.

6.7.2 Parallel Inductors and the Admittance Chart

In many applications, the transducer radiating area is determined by external factors such as the need to minimize acoustic diffraction or to optimize the deflection of a laser beam. Thus, it is generally not possible to choose the area so that the radiation impedance is 50 Ω. Further, use of a high dielectric transducer, such as lithium niobate, requires extremely small areas at frequencies above 1 GHz to produce an $\hat{R}_a$ of 50 Ω.

Example 6.3. Consider the $LiNbO_3$ on GaP A/O device at 1 GHz in which the area is required to be 8.8×10^{-8} m^2. The characteristic is shown in Figure 6.19. In this case, the resistance at resonance is only about 10 Ω. Addition of a series inductor, either as a bond wire or as an external element, will only serve to move the characteristic onto the inductive portion of the chart. It is, however, possible to decrease the reflection coefficient of the device by the addition of a parallel inductor, as shown in Figure 6.19. In this figure, the Smith chart is being used as an *admittance*

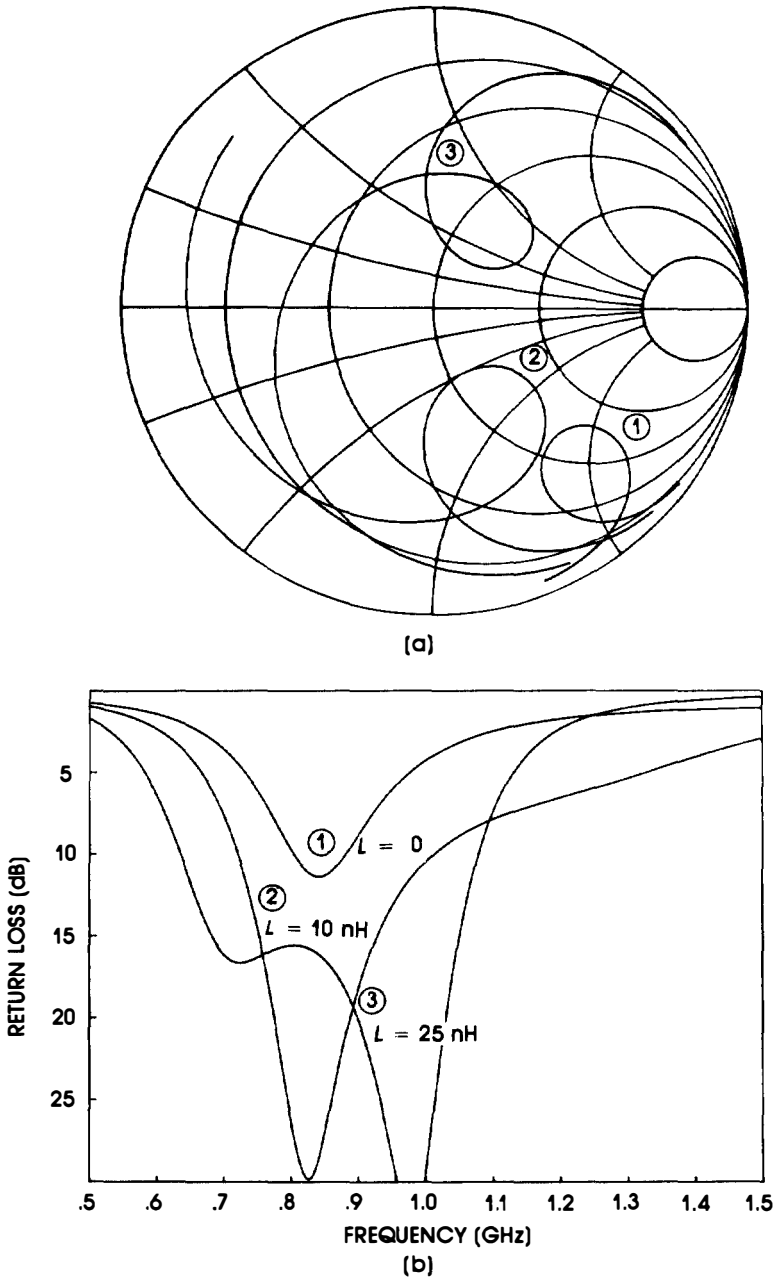

Figure 6.18 Use of series inductor as a matching element: curve 1; L = 0; curve 2; L = 10 nH; curve 3; L = 25 nH. These inductances are higher than can be supplied by bond wires.

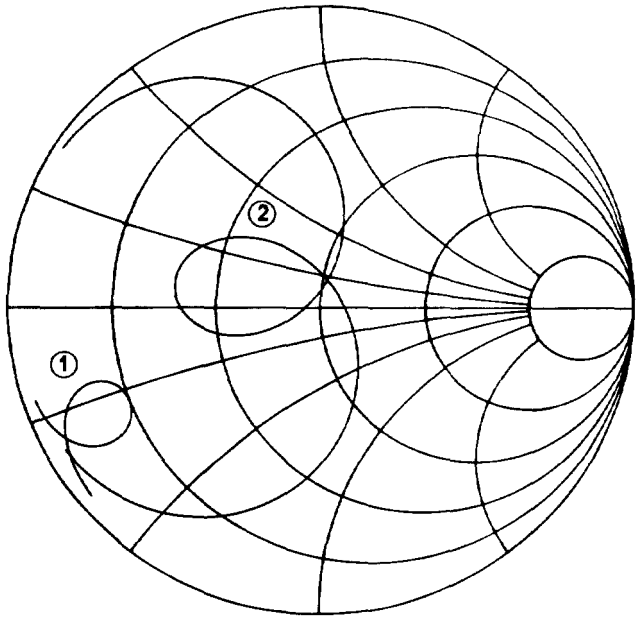

Figure 6.19 If the radiation resistance is between 10 to 20 Ω, a parallel inductor usually increases device performance: curve 1; the unmatched device; curve 2; the same device with a parallel inductor of 3×10^{-9} H.

chart. The constant-resistance circles are transformed to constant-conductance circles; a parallel inductor moves the characteristic along one of these circles. Because for high frequency operation the characteristic is usually located in the lower left portion of the chart, a parallel inductor will generally improve the device performance. If the area is extremely large so that $\hat{R}_a$ is very low (e.g., $< 5\ \Omega$), reducing ρ will probably require the design of a more complex matching network involving multiple elements or the use of multiple radiating elements.

6.8 SERIES AND PARALLEL CONNECTIONS OF ACOUSTIC RADIATORS

There are a number of important acoustic structures in which the radiation resistance is very small. This small resistance may be due to a large C_0 or to a small coupling constant. The clamped capacitance is large when high permittivity transducers (such as lithium niobate) operating at very high frequencies are used, or when the radiation area is required to

be very large, as in certain high-performance A/O devices. Moderate or low coupling transducers, such as sputtered ZnO or vapor-deposited CdS are quite useful at very high frequencies. These materials have relatively low permittivities compared with $LiNbO_3$, but a k_t of typically less than .3. In both situations, the capacitive reactance dominates the small resistive component, and the device looks nearly like a short circuit at high frequencies. Addition of a parallel inductor will reduce the reflection coefficient only marginally or not at all. A sophisticated multielement matching network could be designed, but a more practical solution for this structure is to attempt to increase the radiation resistance by breaking the transducer into distinct radiating elements that are connected in series, as shown in Figure 6.20.

If there are N (assumed identical) radiating elements, the clamped capacitance is equal to C_0/N, and thus the radiation resistance is *multiplied* by N (5.59). If the number of elements increases, the radiating area of each element may also increase without adversely affecting the radiation resistance. An added advantage of increased area is the decreased acoustic intensity, which results in fewer nonlinearities. If the elements are spaced closely together, they can act as a phased grating, which results in the ability to change the angle of propagation as a function of frequency. We will return to this property in Chapter 8.

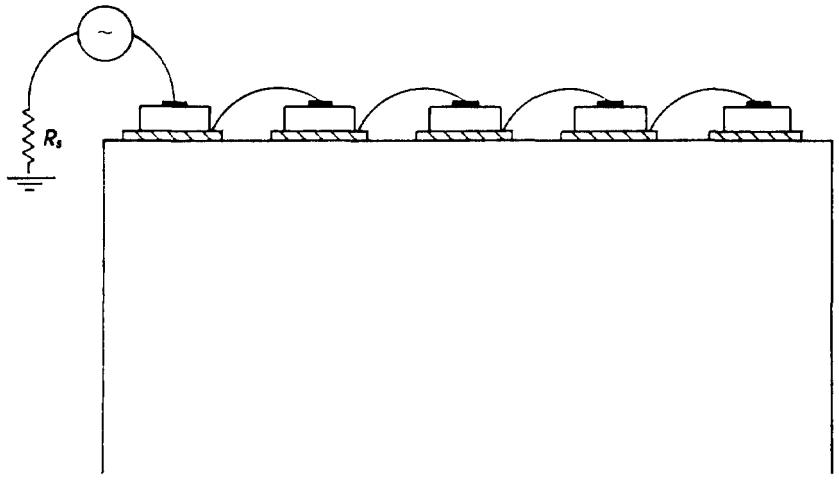

Figure 6.20 A series connection of acoustic radiators reduces C_0 by a factor of N, where N is the number of radiators, and thus increases the radiation resistance.

A disadvantage of the technique is the added fabrication complexity it introduces. The technique is not a panacea for all problems, because simply increasing the radiation resistance does not automatically ensure efficient wideband operation, especially if the electromechanical coupling is weak. Multiple elements have been used with single-crystal transducers such as lithium niobate or sputtered zinc oxide. An alternative technique, applicable only with sputtered piezoelectric materials, is the deposition of multiple piezoelectric layers. Each piezolayer is separated by metallic layers forming a series connection of capacitors. Again, the net effect is to decrease the net clamped capacitance and to increase the radiation resistance, even though the coupling constant is quite low. With this technique, acoustic waves with frequencies greater than 90 GHz have been excited in sapphire at liquid nitrogen temperature [8].

Example 6.4 In this example, we consider the design of a wideband acoustic device consisting of $\langle x \rangle$ $LiNbO_3$ on $-54°$ $\langle y \rangle$ $LiNbO_3$ in which the pure shear mode is excited. Frequency operation is from 2 to 3 GHz, and the area is required to be 8.8×10^{-8} m^2. This is another example of an important A/O device that we will study in more detail in Chapter 8. Even though the same material is used for transducer and substrate, the impedance ratio $Z_T/Z_S = .74$. The high permittivity of $LiNbO_3$ for $\langle x \rangle$-cut (44), its low shear velocity, large area, and high operating frequency (the transducer thickness is typically less than 1 μm) result in a large C_0 and a very small radiation resistance. The ground plane thickness should be as thin as possible to reduce its loading (especially if gold is used). Any increase in the metalization requires a decrease in the transducer thickness. The characteristic is shown in Figure 6.21, in which 4000Å of gold is used as the ground plane. The double-loop structure is due to the gold metalization. Also shown in Figure 6.21 is the same structure, in which four and eight radiating elements, each of area 8.8×10^{-8} m^2, are connected in series. The radiation resistance in this configuration is large enough so that a single parallel inductor can be used to efficiently match the device.

Finally, we consider a *parallel* connection of radiating elements. If all elements are of equal area, the effect is to increase the clamped capacitance and to lower the radiation resistance. If, however, the radiating elements have different thicknesses, a dramatic increase in acoustic bandwidth can be achieved. This is the case of a *wedged* transducer, as shown in Figure 6.22. Such structures are relatively easy to fabricate with single-crystal technology, but are quite challenging if sputtered transducers are used. They can be modeled by breaking up the radiating area into a series of parallel connected elements, each with a different thickness (as shown in Figure 6.22b). Figure 6.23 shows the parallel connection of four radiating

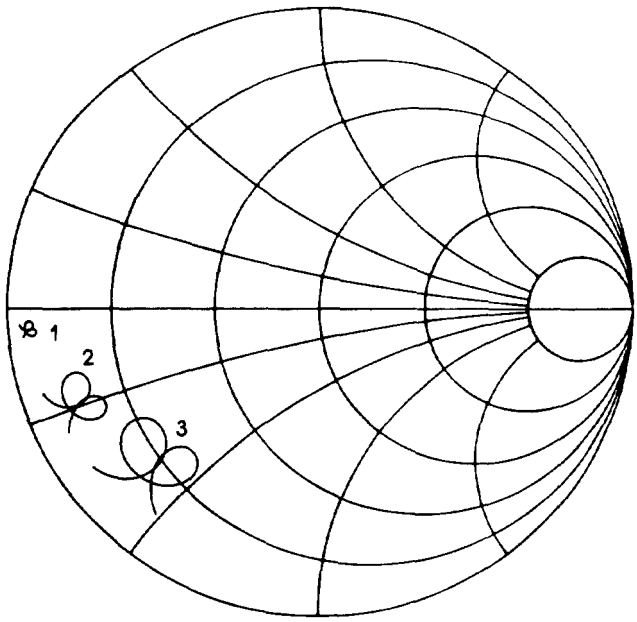

Figure 6.21 Improvement in device performance using series connected radiating elements. *Note*: Curve 1, $\hat{R}_a = 3\ \Omega$; curve 2 (4 elements), $\hat{R}_a = 6\ \Omega$; curve 3 (8 elements), $\hat{R}_a = 12\ \Omega$.

elements with a linear variation in thickness. Devices that have been fabricated with wedged transducers generally show significantly "tighter" impedance characteristics, which facilitates matching.

6.9 USE OF THE GROUND PLANE AS A MATCHING ELEMENT

Now we return to Example 6.2 in which an (x)-cut lithium niobate transducer is bonded to the quasi slow shear mode in paratellurite. In this case, in which there is a severe impedance mismatch between transducer and substrate, we can achieve a significant improvement in bandwidth by using the metallic bond layer as a quarter-wave transformer. This strategy is analogous to the use of an antireflection coating in optics. For a perfect

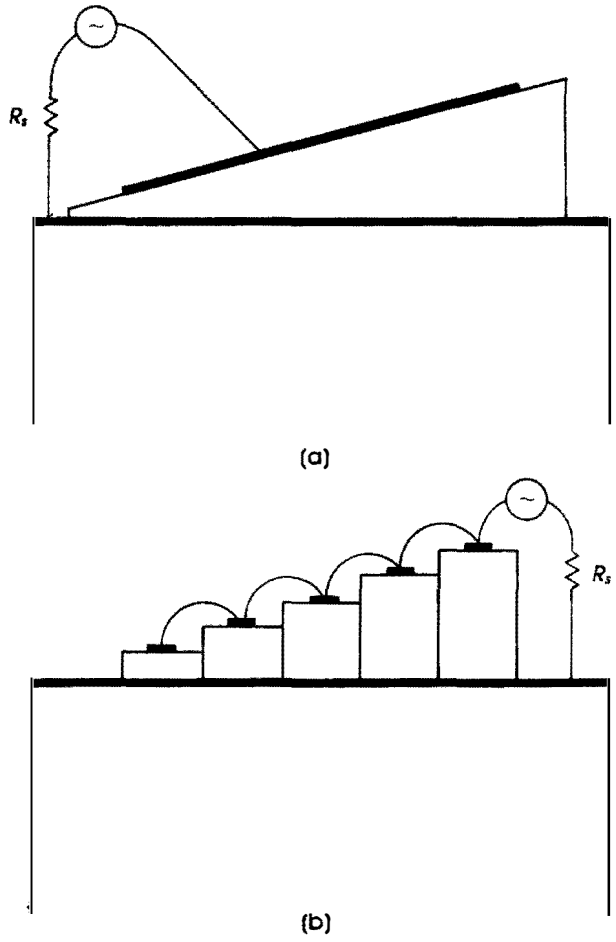

Figure 6.22 Wedged transducer: (a) represents the cross section of the transducer; (b) represents the model using a parallel connection of radiators of varying thicknesses.

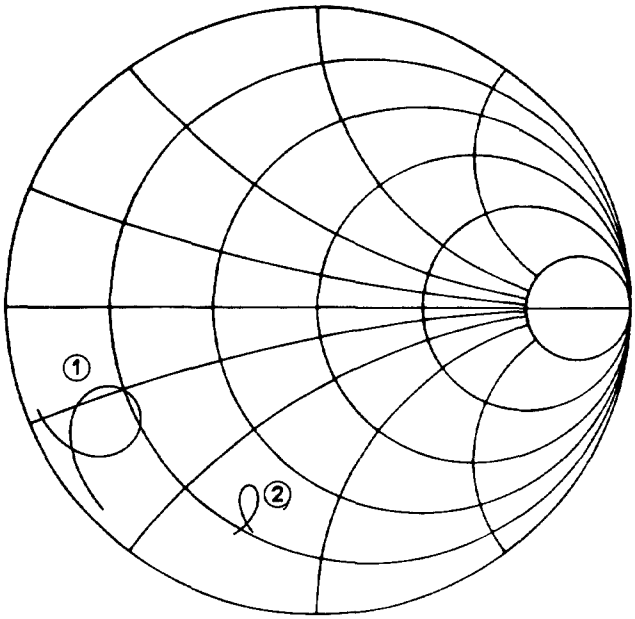

Figure 6.23 Improvement in performance using wedged transducer: curve 1; a typical characteristic with no matching elements; curve 2; the same characteristic broken up into four parallel radiators with thicknesses from 1.5 to 2.5 μm.

match, the required impedance is

$$Z_m = \sqrt{Z_S Z_T} \tag{6.19}$$

where Z_m is the *acoustic* impedance of the metallic bond layer. Substituting values for the substrate and transducer into (6.19) from Table 6.2, we see that indium is very nearly a perfect match between the lithium niobate transducer and the paratellurite, although tin has also been successfully used. The optimal thickness required is a quarter wave:

$$\frac{\lambda}{4} = \frac{v_a}{4f} = \frac{1.3 \times 10^3}{4 \times 50 \times 10^6} = 6.5\ \mu\text{m}$$

Figure 6.24 shows the impedance and return loss with the quarter-wave "matching." Compare this characteristic with that of Figure 6.8. The bandwidth has been increased to over 60% without the use of any external elements.

Finally, Figure 6.25 shows the same device with the 200-nH series inductor. In this case, the bandwidth has been increased to almost 75%.

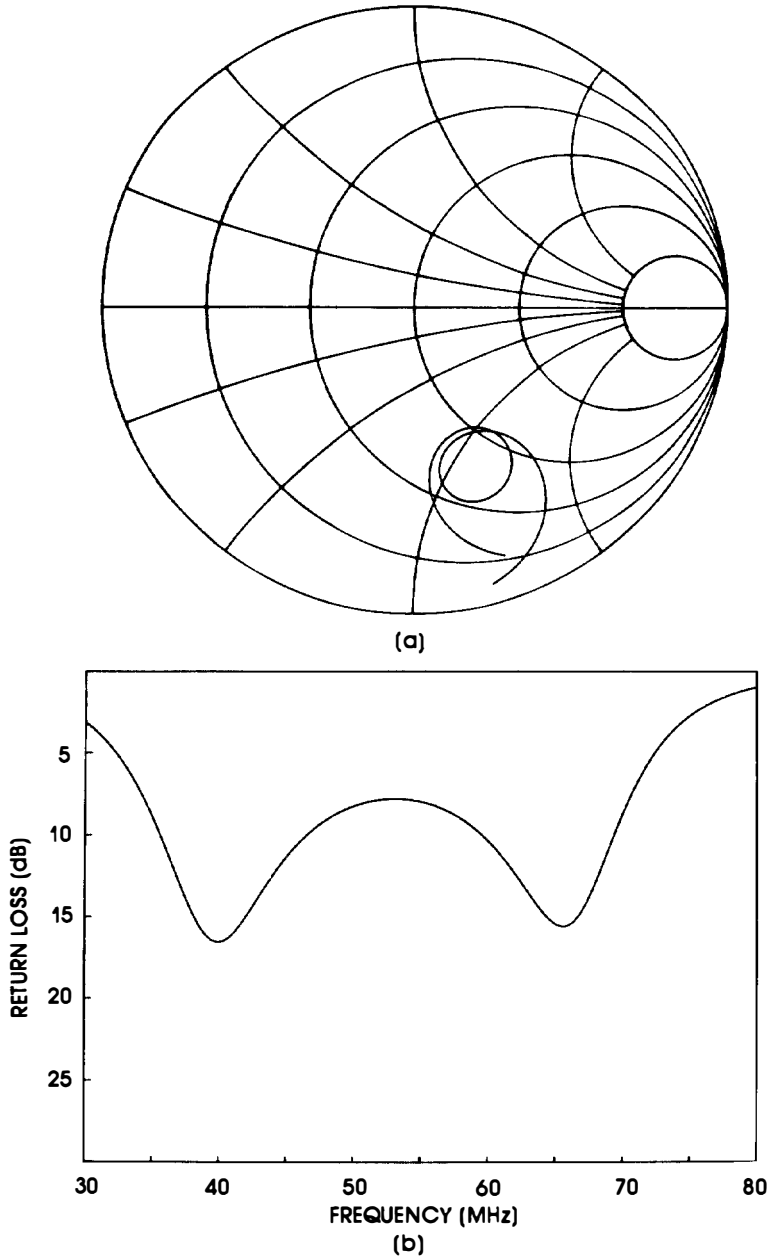

Figure 6.24 Use of the ground plane as a quarter-wave transformer. The parameters are given in Figure 6.8 for the shear lithium niobate on paratellurite. The ground plane is 6.5 μm of indium, which is nearly a perfect match between the high transducer impedance and the low substrate impedance.

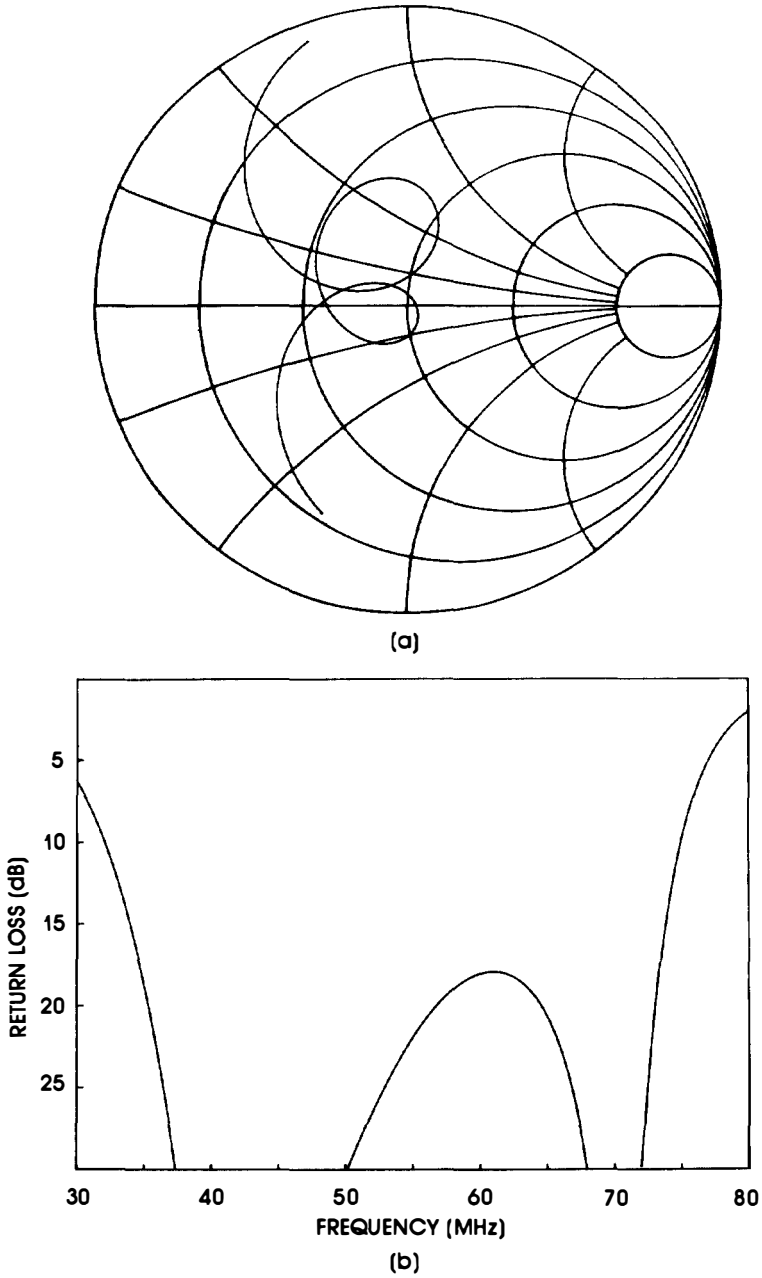

Figure 6.25 Use of ground plane and series inductor in the lithium niobate–paratellurite device increases the bandwidth to nearly 75%.

The only potential problem in this approach is the difficulty of depositing precisely the required indium thickness (3.25 μm per surface). In summary, low frequency operation allows the transducer active area to be relatively large, and ground layer effects are minimized. If the impedance mismatch is large, a ground metalization of proper thickness can act as a quarter-wave transformer and significantly increase the bandwidth. In high frequency operation, the active area must be reduced dramatically. Careful attention must be given to the mismatch between transducer and ground metalization. External matching elements are usually required.

PROBLEMS

6.1 Plot the impedance characteristic on the Smith chart for a circuit consisting of a parallel combination of a resistor and inductor.

6.2 Plot the return loss for the circuit of Problem 6.1

6.3 Derive (6.14) by applying the stressfree condition to the equivalent circuit shown in Figure 6.9.

6.4 Use the program of Figure 6.12 to plot the input characteristic of the device of Example 6.1 ($LiNbO_3$ 36° ⟨y⟩ on $LiNbO_3$ longitudinal) operating at 2 GHz using .5 μm of gold as the ground metalization. Increase the attenuation of the gold in the program to 10^4 and note the effect on the impedance. Explain.

6.5 Plot the impedance characteristic for the device of Example 6.1, using an aluminum ground plane of .2 μm.

6.6 Repeat Problem 6.5 using silver.

6.7 Discuss the effect of varying k_t and transducer area A by the size of the resonance loop in Example 6.2.

6.8 Show that the mechanical-to-electrical transformation ratio ϕ can be written as

$$\phi^2 = h^2 C_0^2 = \frac{Z_T v_a C_0}{d} k_t^2$$

REFERENCES

1. S. Ramo, T. Whinnery, and T. Van Duzer, *Fields and Waves in Communication Electronics,* 2nd Ed., John Wiley, and Sons, New York 1984 Chapter 5.
2. A. Ballato, *Transmission-Line Analogs for Piezoelectric Layered Structures,* Ph.D. dissertation, Polytechnic Institute of Brooklyn, 1972.
3. T. Reeder and D. Winslow, "Characteristics of Microwave Acoustic Transducers for Volume Wave Excitation," *IEEE Trans. Microwave Theory and Tech.* **MTT-17** (11), 927 (1969).
4. R. Moore, R. Sundelin, G. Borsuk, J. Lane, C. Huber, and S. Lieberman, "Broadband Low Triple Transit Microwave Delay Line," *Proc. IEEE Ultrasonics Symposium,* 193 (1978).
5. J. deKlerk, "Multilayer Thin Film Piezoelectric Transducers," *IEEE Trans. Sonics and Ultrasonics* **SU-13** (3) 99 (1966).
6. K.C. Gupta, R. Garg, and R. Chadha, *Computer Aided Design of Microwave Circuits,* Artech House, Norwood, MA, 1981.
7. T. Noguchi and A. Fukumoto, "Diagnostic Study of Bonded, Thickness Mode Transducers by Input Impedance Measurement," *IEEE Trans. Sonics and Ultrasonics* **Su-20** (4), 365 (1973).
8. B. Hadimioglu, *et al.*, "High Efficiency, Multiple Layer ZnO Acoustic Transducers at Millimeter-Wave Frequencies," *Applied Physics Letters* **50** (23) 1642 (1987).